ELSEVIER

Journal of Hazardous Materials 62 (1998) 211–230

JOURNAL OF HAZARDOUS MATERIALS

Pore-scale investigations on vibratory mobilization of LNAPL ganglia

Lakshmi N. Reddi *, S. Menon, A. Pant

Department of Civil Engineering, Seaton Hall, Kansas State University, Manhattan, KS 66506, USA

Received 6 March 1998; revised 12 May 1998; accepted 13 May 1998

Abstract

Light nonaqueous-phase liquid (LNAPL) pools formed at the interface of unsaturated and saturated zones fluctuate with groundwater table and form a 'smear zone' occupied by ganglia or blobs. Recovery of these residual ganglia has always been the most difficult component in subsurface remediation. Previous experimental studies, conducted at laboratory-scale, concluded that localized vibrations are effective in mobilizing LNAPL ganglia. In this paper, results from a pore-scale investigation on vibratory mobilization of LNAPL ganglia are presented. The objective of this investigation was to quantitatively evaluate the extent of ganglia mobilization and to assess the role of overburden stress on vibratory mobilization. The paper is organized into three parts. First, the mobilization of a solitary ganglion in a porous medium subjected to vibrations is tracked using micromodel experiments and image analyses. Direct visualization of momentary particle rearrangement became possible through these experiments. Mobilization, break-up, and coalescence processes were observed at the scale of a single ganglion. Increased overburden stress at greater depths was found to hinder ganglia mobilization. In the second part, mobilization of a population of ganglia under the influence of vibrations is analyzed using results from darcy-scale experiments. These results confirmed the role of overburden stress and indicated that the processes of coalescence and break-up might be occurring only locally without impacting the size distribution of ganglia population at sample scale. In the third part, a mathematical framework is suggested to model the transport of ganglia population under the influence of vibrations. A convection-type equation is used to represent the transport of ganglia population. The effect of vibrations was incorporated using space-dependent probabilities for ganglia stranding.

Keywords: Vibratory mobilization; Recovery of LNAPL ganglia

* Corresponding author. Tel.: +1 785 532 1586; fax: +1 785 532 7717; e-mail: reddi@ce.ksu.edu

0304-3894/98/$ - see front matter
PII: S0304-3894(98)00164-2

1. Introduction

Light nonaqueous-phase liquids (LNAPLs), when spilled on the ground in sufficient quantities, can migrate downward through the unsaturated zone, and form a pool at the groundwater table. When the water table fluctuates because of pumping or recharge operations, the LNAPL pool follows the watertable. During the movement of the pool, a 'smear zone' is formed because of the entrapment of the LNAPL in the form of blobs or ganglia as a result of capillary forces. The residual saturation of the LNAPL (fraction of the LNAPL volume to the pore volume) thus contained in the smear zone in the form of ganglia may be as large as 50% [11]. These ganglia dissolve slowly and constitute a long-term threat to groundwater resources. Unlike the pool, which is a free product of the LNAPL, the ganglia are difficult to recover. It has been well established that pump-and-treat processes can not provide hydraulic gradients large enough to overcome the capillary forces trapping the ganglia within the pore spaces [21]. Development of in situ remediation schemes, based on physical, chemical, and biological processes, to recover the LNAPL ganglia has been an active area of research interest in the recent past.

Reddi [18] reported an exploratory study documenting the feasibility of mobilizing LNAPL ganglia by inducing localized vibrations in the contaminated soils. The intent of vibratory mobilization was to mobilize the entrapped ganglia in a controlled manner to the point of intended collection. It was intended to serve as a pretreatment process followed by other methods such as bioremediation and air sparging. A field implementation scheme similar to vibroflotation, a process used to densify subsurface soils [1,4], was conceived in that study to recover residual NAPL ganglia. Subsequent studies [19,20] attempted to identify the mechanisms involved in vibratory mobilization of LNAPL ganglia. Reddi and Challa [19] conducted laboratory-scale experiments which involved vibrating NAPL-contaminated soil columns on a shaking table at various amplitudes. Recoveries up to 88% of the entrapped residual saturations were observed in that study. The role of soil compaction and dilation on LNAPL recoveries was demonstrated, and the enhancement in recoveries as a result of augmenting vibrations with viscous forces (by providing flow gradients during vibrations) was also established.

Reddi and Wu [20] used a similar experimental approach to conclude that momentary particle rearrangement was the primary mechanism underlying vibrorecovery of LNAPL ganglia from sands. However, this conclusion was based on indirect observations. A comparison was made between the recoveries observed from soil columns subjected to vibrations and those expected under viscous conditions alone. The estimates of gradients required to recover 60% of the trapped LNAPL ganglia from sands using viscous forces alone are shown in Fig. 1, as a function of intrinsic permeabilities. These estimates were based on studies by Wilson et al. [21] who summarized results from a number of experimental investigations involving glass beads, soils, and a variety of immiscible liquids. Also shown in Fig. 1 are the results from an experiment involving vibration of sand columns, which resulted in 69% recovery of trapped ganglia. The vibrations compacted sandy soils resulting in a reduced intrinsic permeability (from 'A' to 'B'). It appeared that the 69% recovery achieved in the experiments with vibrations could not be explained by mere consideration of viscous forces. This indicated that momentary

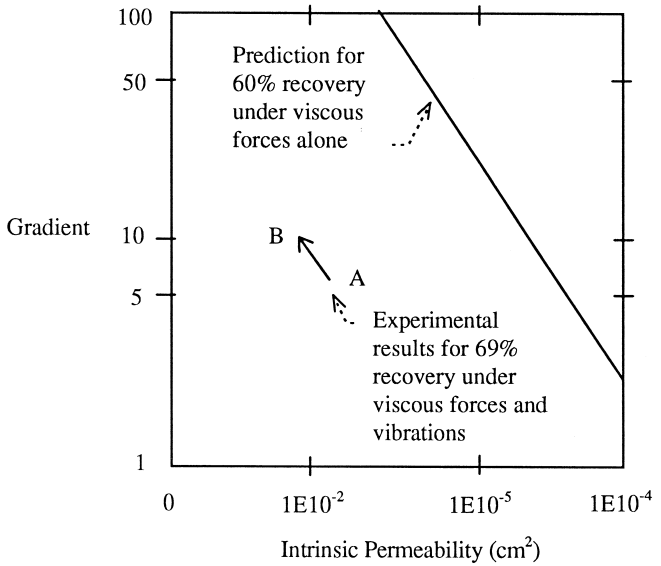

Fig. 1. Comparison of experimental conditions and corresponding recoveries observed in experiments with vibrations and those estimated by Wilson et al. [21].

particle arrangement *during* vibrations was the predominant mechanism for vibratory mobilization of ganglia from sands.

The objective of the studies described above was to develop an understanding of the practical implications of vibratory mobilization. Optimization of recoveries, design, and construction of an in situ vibrator probe, were among the issues addressed in those studies. In this paper, results from a pore-scale investigation are presented in an attempt to understand the behavior of a solitary ganglion and that of a population of ganglia. The underlying objective of this pore-scale investigation was to quantitatively evaluate the extent of ganglia mobilization and to assess the role of overburden stress on vibratory mobilization. These are important considerations in planning and design stages of field scale implementation of vibrorecovery.

There have been several studies on the pore-scale processes involved in ganglia entrapment. Chatzis et al. [2] provided some of the earliest visual observations on magnitude and detailed structure of residual oil saturation. Using photofabrication and etching techniques, they created several 2-D patterns of pore networks of variable pore size and pore interconnectedness within a glass material. The effects of pore structure on residual saturation were discussed in their study. An approach used by Yadav et al. [22] quantified organic liquid distribution at the pore scale using photomicrographs of polished sections of sandstone containing residual organic liquid. Conrad et al. [3] visually observed the organic phase and concluded that the size, shape, and spatial distribution of residual organic ganglia significantly affect their dissolution into the water phase and their biotransformation. Hornof and Morrow [7] investigated the effects of interfacial tension on displacement behavior through flow visualization experiments

in thin layers of sintered glass beads. Efforts have also been made to correlate the residual ganglia characteristics to porous medium characteristics [9,10]. The ganglion length and volume distribution were obtained as a function of porous medium size for a series of uniform porous media. They also generated representative elementary volumes (REVs) for residual saturation using Monte Carlo procedure. Powers et al. [17] used similar experimental means to observe the ganglia at pore-scale for the sake of studying the mass transfer rates at the interface of the immiscible and miscible phases. In contrast to the experimental investigations, very few studies addressed modeling of the transport of ganglia population. Payatakes et al. [16], Payatakes [15], and Ng and Payatakes [14] provided one of the few conceptual bases to simulate oil ganglia motion, partition, and coalescence during immiscible displacement. They used birth and death processes to develop a system of advection–dispersion type equations, and solved them for the number of moving and stranded ganglia. Conducted in the context of enhancing oil recoveries in petroleum engineering, these studies provided a basis for the mathematical framework of the present study, as discussed later. More recently, Lowry and Miller [8] conducted a pore-scale modeling study, using a random network approach, to investigate factors affecting residual phase in strongly wet, capillary-dominated systems. Porous media were modeled as three-dimensional networks of pore bodies and throats.

The work reported in this paper contributes to the literature by extending the above pore-scale studies to porous media subjected to vibrations. The paper is organized into three parts. In the first part, observations from micromodel experiments are presented and the behavior of a solitary ganglion is discussed. In the second part, results from darcy-scale experiments are presented to show the behavior of a population of ganglia. In the third part, a mathematical basis is presented to model the transport of ganglia under the influence of vibrations.

2. Behavior of a solitary ganglion under the influence of vibrations

2.1. Experimental materials and methods

The micromodel set-up consisted of a Plexiglas chamber with dimensions 280 mm $\times$ 213 mm $\times$ 10 mm. The chamber has three inlet ports at 25 mm from the bottom and three outlet ports 25 mm from the top. In addition, nine small ports were provided at three different depths, ‘top’, ‘middle’, and ‘bottom’ for the purpose of injecting the LNAPL with a syringe through a cork stopper. As shown in the schematic of the experimental set-up (Fig. 2), the chamber was situated firmly using clamps on a vibrating table (FMC Model: VP51D1) (50 cm $\times$ 50 cm) that could be vibrated at 3600 rpm. The amplitude of vibrations was controlled by means of a dial ranging from zero to 10 with the greatest setting corresponding to an amplitude of 0.6 mm. The inlet ports of the chamber were connected to a computer-controlled pump which enabled an adjustable and a controlled flow rate of water. Two of the injection ports, one at the top and the other at the bottom of the chamber, were connected to burettes to monitor the constancy of the head difference of water. Once the LNAPL was injected into the chamber, its

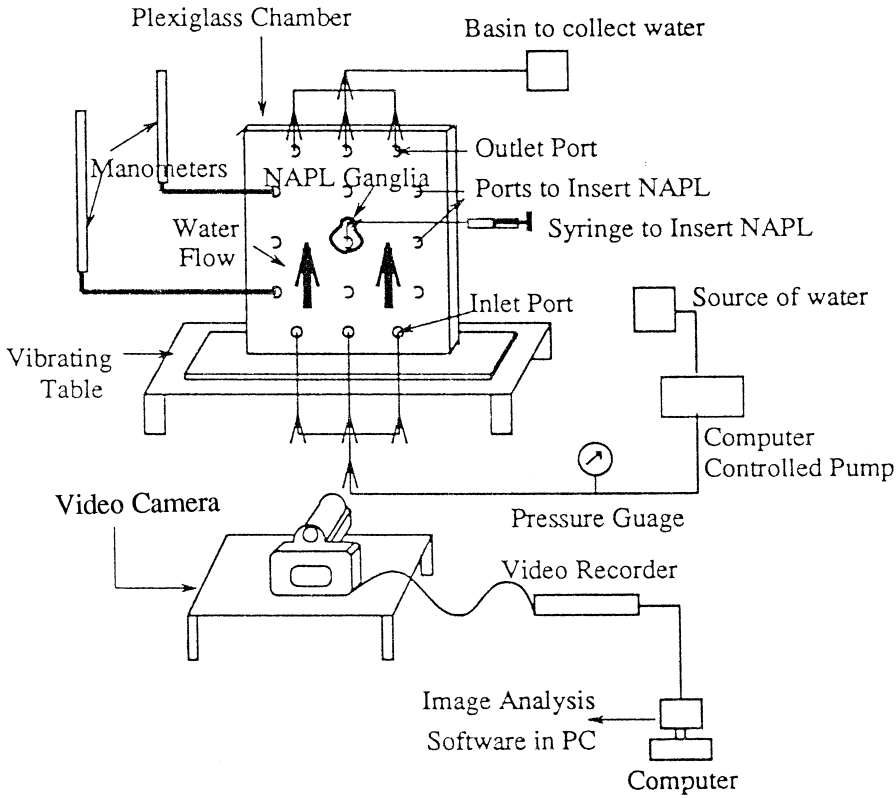

Fig. 2. Schematic of experimental set-up for micromodel experiments.

behavior was monitored using a video camera (with a macrolens) which was connected to a VHS player. This enabled a simultaneous viewing and recording of the experiment. A video capturing card (Video Blaster) installed in the computer provided a video interface for the PC. The video was then converted to frames of image data that could be displayed sequentially. The computer allowed data capture at the rate of 5 frames s^{-1}. This rate of data capture was felt adequate to observe the momentary changes of ganglion shape and size during vibrations. The data were then analyzed using Sigma Scan, an image analysis software developed by Jandel Scientific.

After a number of trial experiments (conducted to improve visualization), uniform-sized glass beads of 2-mm diameter were chosen as the porous medium. The beads were manufactured by Jaygo, NJ. The immiscible liquid used to simulate the LNAPL was Soltrol, a mixture of Isoparaffins, manufactured by Phillips-66. Soltrol was used in a number of prior laboratory studies [20,21]. It was chosen in this study primarily because of its negligible solubility in water, mild odor, and low volatility, which made it safe to work with. To enhance the videography, Soltrol was dyed with a drop of DuPont Oil Red B liquid, which was a mixture of aromatic hydrocarbons-xylene, ethylbenzene, benzene and 2-napthalennol azo alkyl derivatives.

The experiments were begun by first filling the chamber with water, and then pouring the glass beads using a funnel to form a porous media free of air pockets. Two types of experiments were conducted. In the first type, the pore structure was recorded before, during, and at the end of vibrations by focusing on a 1 cm × 1 cm window at nine locations close to the nine injection ports of the chamber. In the second type of experiments, a small volume of Soltrol, sufficient enough to be visualized, was injected into the water-saturated beads at top, middle, or bottom ports and its shape and size were monitored continuously.

2.2. Results and discussion

Prior to vibrating the chamber, about thirty pictures at each of the three levels (top, middle, and bottom) were taken and the distribution of interparticle spacings was obtained using the photographs. The majority of these spacings were between 0.04 and 0.12 mm (Fig. 3). To record fluctuations in pore and throat dimensions during the application of vibrations, a 10 mm × 10 mm viewing window was chosen at a point about 100 mm below the top of the chamber, which fell in between the 'top' and 'middle' levels of the chamber. The changes to the pore structure in this fixed window were recorded and analyzed. Three representative frames of the window are shown in Fig. 4. The beads were labeled to keep track of the pore dimensions which were marked by the white lines. All of the tracked dimensions enlarged during the time period of 8.4 s. The distinction between a 'pore' and a 'throat' was lost at times (see the interparticle spacing between beads 2 and 3).

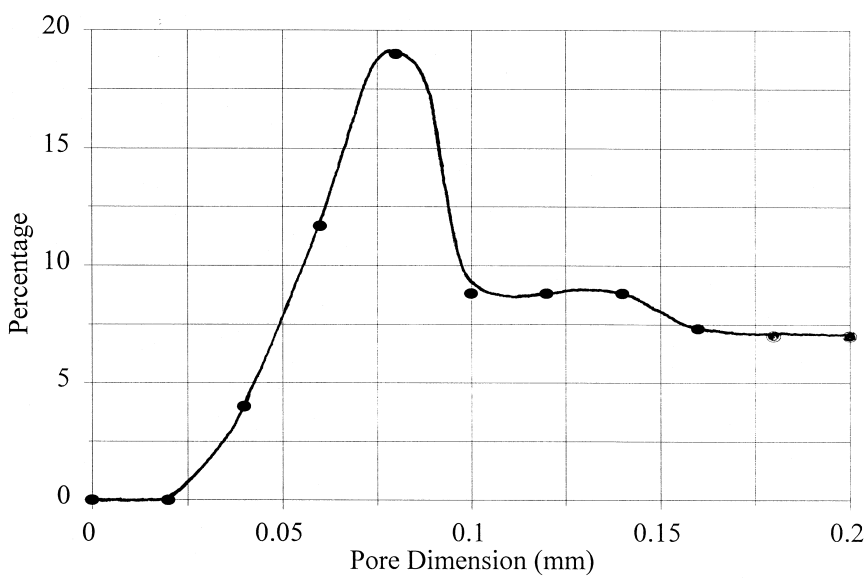

Fig. 3. Distribution of pore dimensions before vibrations.

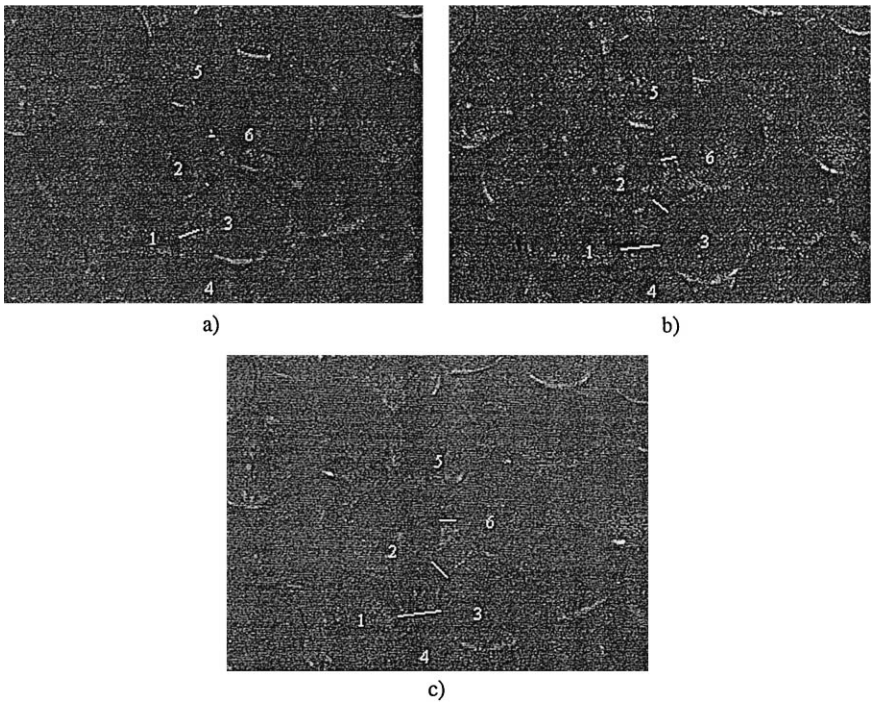

Fig. 4. Representative frames of pore structure during vibrations, a) at time t, b) at time $t+3.8$ s, and c) at time $t+8.4$ s.

At the amplitude setting of 4, about six such dimensions were tracked for a time period of about 9 s (Fig. 5). It should be noted that the six dimensions represented here were not captured during the same time interval, but the period of capture was the same for all of them (except for No. 1). The results reflected a continuous change of the dimensions with pore constriction and enlargement occurring successively. Pore throats which were initially smaller than 0.1 mm, momentarily enlarged up to 0.4 mm. It is interesting to contrast this with the condition of pore structure at the end of vibrations. The distribution of interparticle spacings obtained by analyzing windows at the end of vibrations (amplitude setting: 4) is shown in Fig. 6. The majority of the spacings were within 0.025 and 0.10 mm with no dimension greater than 0.1 mm. Thus, the end condition of pore structure was not at all representative of the pore changes during vibrations, and the momentary changes during vibrations were significant. The same trends were observed at the other amplitude settings of 5 and 6 where the momentary particle spacings increased to a maximum of 1.5 mm.

The fate of a solitary ganglion was then examined by injecting a blob of Soltrol, about 5 ml in volume, at top, middle, and bottom of the chamber. Representative frames (Fig. 7) demonstrated the fate of a ganglion situated at the top of the chamber and subjected to an amplitude setting of 4. The breakup of parent ganglion was apparent in these frames. The parent ganglion remained stranded even after a time period of 50 s,

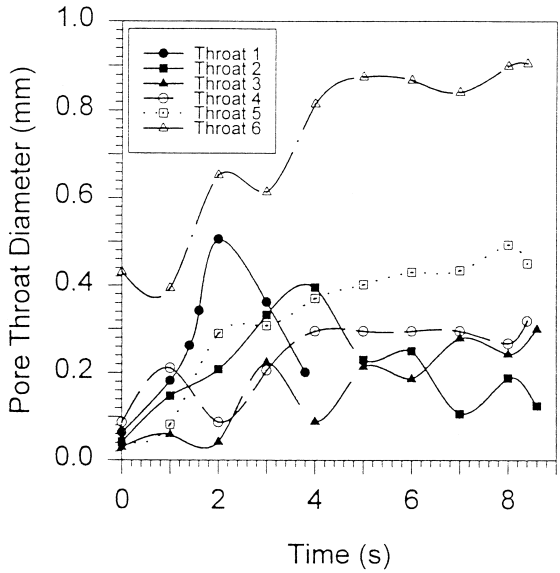

Fig. 5. Variation of six representative pore dimensions during vibrations.

whereas the daughter ganglion escaped the viewing window after about 20 s. Image analyses on the parent ganglion showed that the bottom-most point of the ganglion remained at the same location whereas the centroid of the ganglion moved upward by

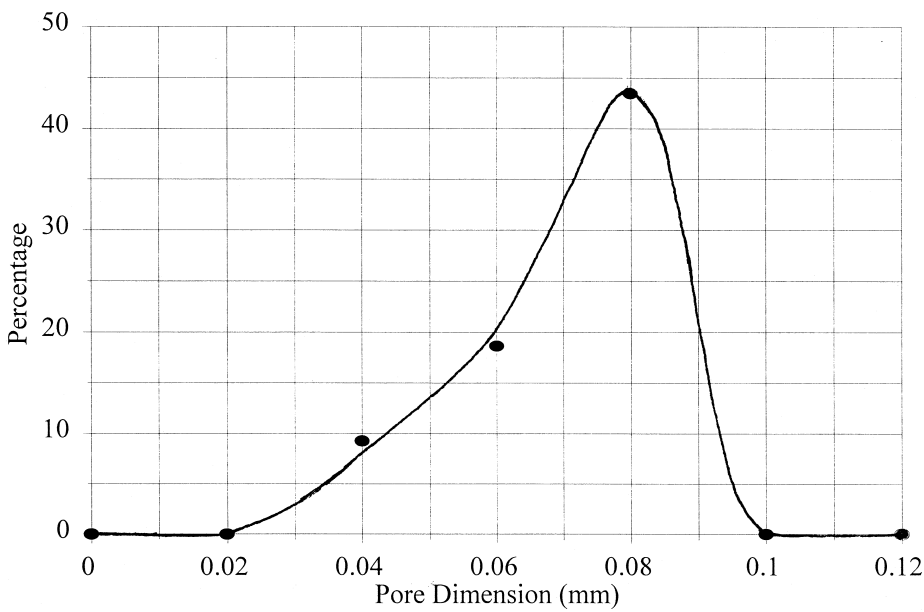

Fig. 6. Distribution of pore dimensions at the end of vibrations.

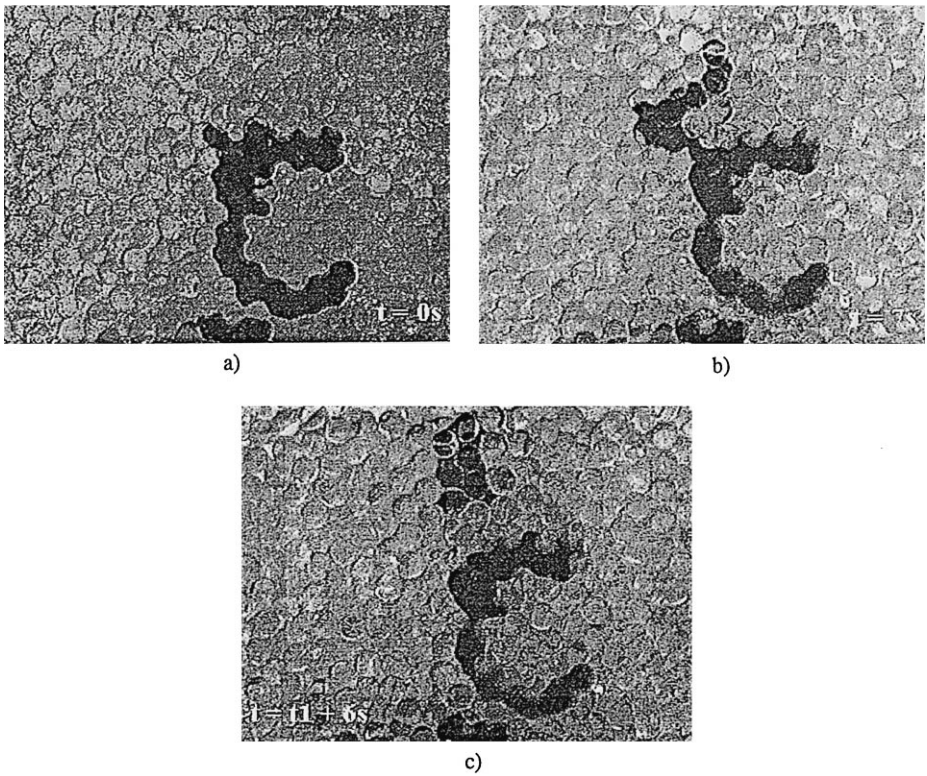

Fig. 7. Fate of a solitary ganglion subjected to vibrations, a) at time $t = 0$ s, b) at time $t = 7$ s, and c) after break-up at time $t = 13$ s.

about 2 mm, indicating stretching of the ganglion. The daughter ganglion on the other hand, moved as a whole, as both the bottom and centroid of the ganglion showed upward movement (Fig. 8). The amplitude setting was increased to 5 when no further mobilization of the parent ganglion was noticed. The parent ganglion was mobilized at this setting, with its centroid and bottom-most point pushed upward by 5 mm in about 40 s, prior to its escaping the window.

Frames analyzed for two other ganglia injected at the middle and bottom of the chamber showed a different behavior. Image analyses of the frames for the ganglion injected at the mid level indicated that the ganglion was constantly undergoing break-up and coalescence. The results of the image analyses (Fig. 9) showed that the bottom-most point of the ganglion did not move, whereas the centroid of the ganglion changed rapidly. A close examination of the frames indicated that the ganglion broke into daughter ganglia at times, and the daughter ganglia coalesced at other times. These processes constantly changed the location of the centroid of the ganglion under consideration. During break-up process, the centroid was brought down, whereas during coalescence, the centroid was moved upward. Results from the image analysis on the fate of ganglion injected at the bottom level of the chamber are shown in Fig. 10. The

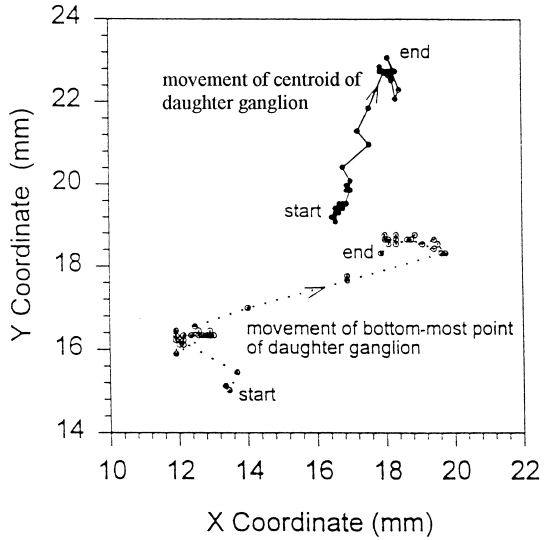

Fig. 8. Progressive upward movement of the bottom most point and the centroid of the daughter ganglion created at the top of the chamber.

centroid of the ganglion remained within about 0.4 mm of its initial location. This small difference could have been the result of slight changes in the shape of the ganglion, and not because of its movement. The bottom-most point of the ganglion remained unaltered. This indicated that the ganglion did not move.

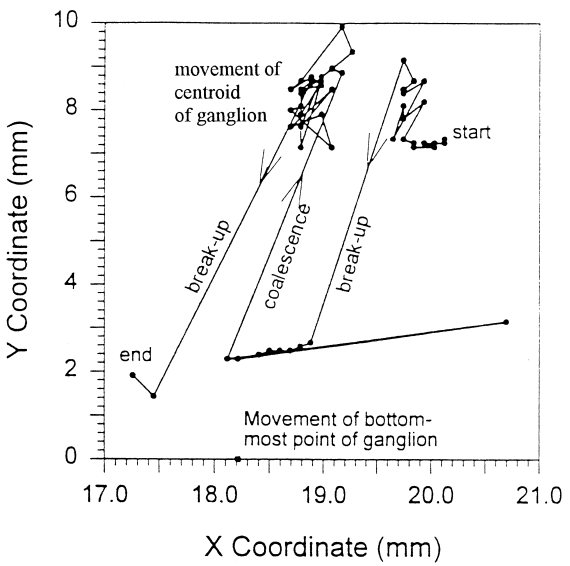

Fig. 9. Movement of the bottom most point and the centroid of a ganglion created at the middle of the chamber.

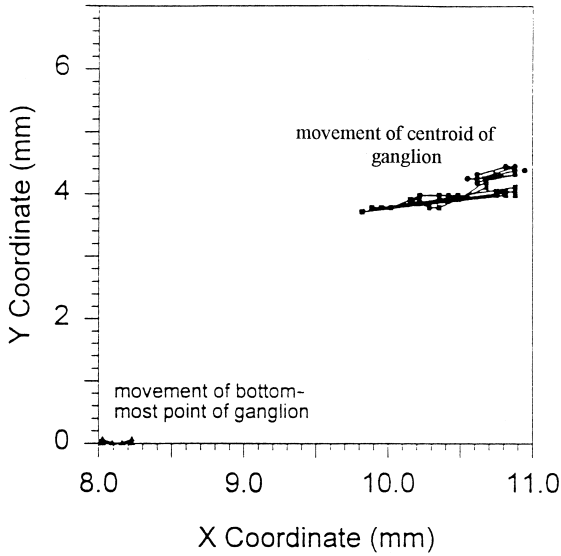

Fig. 10. Movement of the bottom most point and the centroid of a ganglion created at the bottom of the chamber.

The differences in ganglia behavior (at the same amplitude setting of vibrations) between the top, middle, and bottom of the chamber supported the conclusion that the overburden stress played a significant role. At low overburden stresses, the particles seemed to exercise freedom of rearrangement thus altering momentarily the interface (water-immiscible phase) curvatures. These momentary changes resulted in the release of ganglia from pore throats. An increase in overburden stress seemed to restrict particle rearrangement thus preventing ganglia mobilization.

3. Behavior of ganglia population under the influence of vibrations

3.1. Experimental materials and methods

The second laboratory program was designed to study the effect of vibrations on the transport of ganglia as a population. The experiments were conducted in a cylindrical Plexiglas column 40 mm in diameter and 240 mm in height (Fig. 11). The porous media consisted of glass beads (sizes ranging from 2 mm to 0.85 mm) which were poured in a loose state in the column filled with water. Hexadecane was used as the LNAPL in these experiments. The primary reason for selecting Hexadecane was that it has a high melting point (18.2°C) which facilitated solidification of ganglia with water still remaining in the liquid phase. Like Soltrol, its solubility in water and volatility are low. Hexadecane was introduced from the top as shown in Fig. 11, and it was allowed to displace the water in the beads for a sufficient length of time until fluid saturations reach equilibrium. This was indicated by stabilization of fluid levels in both the inflow and outflow burettes. The column was then backflooded with water at the rate of 1 ml/min with the help of a computer-controlled pump to create residual conditions.

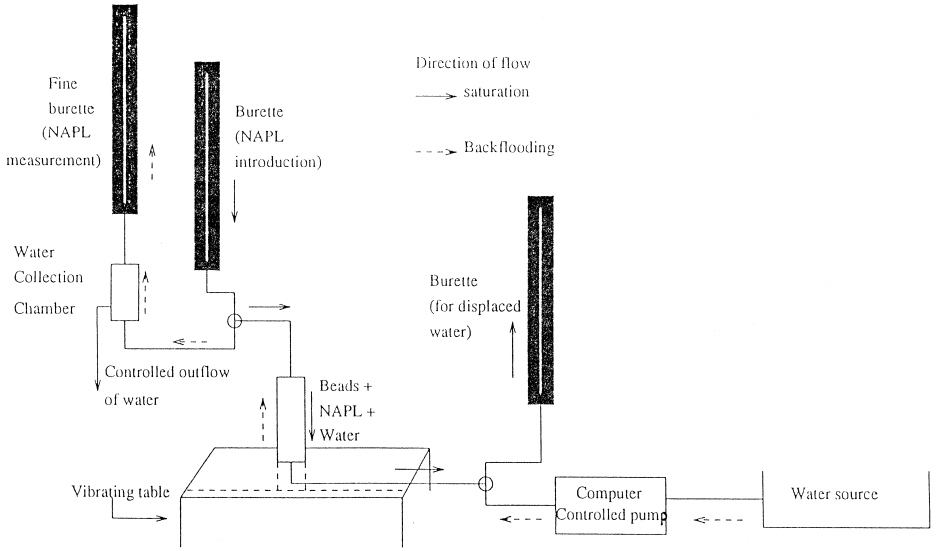

Fig. 11. Schematic of experimental set-up for column experiments on ganglia populations.

The column was subjected to vibrations on the same shaking table used in the experiments discussed in Section 2. The column was vibrated at an amplitude setting of 4 till no recovery was visually noticed. In one of the experiments, simultaneous flow of water at the rate of 100 ml/min was allowed during vibrations to create viscous conditions, and in the other, no flow was imposed to create only buoyancy conditions. To visualize the ganglia, the ganglia were solidified by placing the column in a temperature chamber controlled at 5°C. Hexadecane present in the form of discrete ganglia solidified whereas water remained in the liquid state. The glass beads were then slowly pushed out of the column with the help of a pressure pump and sectioned into three equal parts. The parts were labeled as top, middle, and bottom. The ganglia were separated from the glass beads by placing them in water. The solidified ganglia floated on the top whereas glass beads, being heavier, settled at the bottom. A few ganglia attached to the glass beads were separated by gently rotating the sample in a soil dispersion mixer. The floating ganglia were filtered by passing the sample through a set of sieves. The sieves were weighed with and without the ganglia to determine the weight of ganglia collected on each sieve. A balance with a sensitivity of 0.0001 grams was used. The total weight of the trapped ganglia sorted in the sieves agreed closely with the mass balance estimates. The maximum discrepancy between the two was 4% of the total weight.

3.2. Results and discussion

A comparison of the weights of ganglia retained in the three different sections of the column (Fig. 12) indicated a reduction in the weight of trapped ganglia due to vibrations. It was noticed that all sizes of ganglia were affected by vibrations. The top

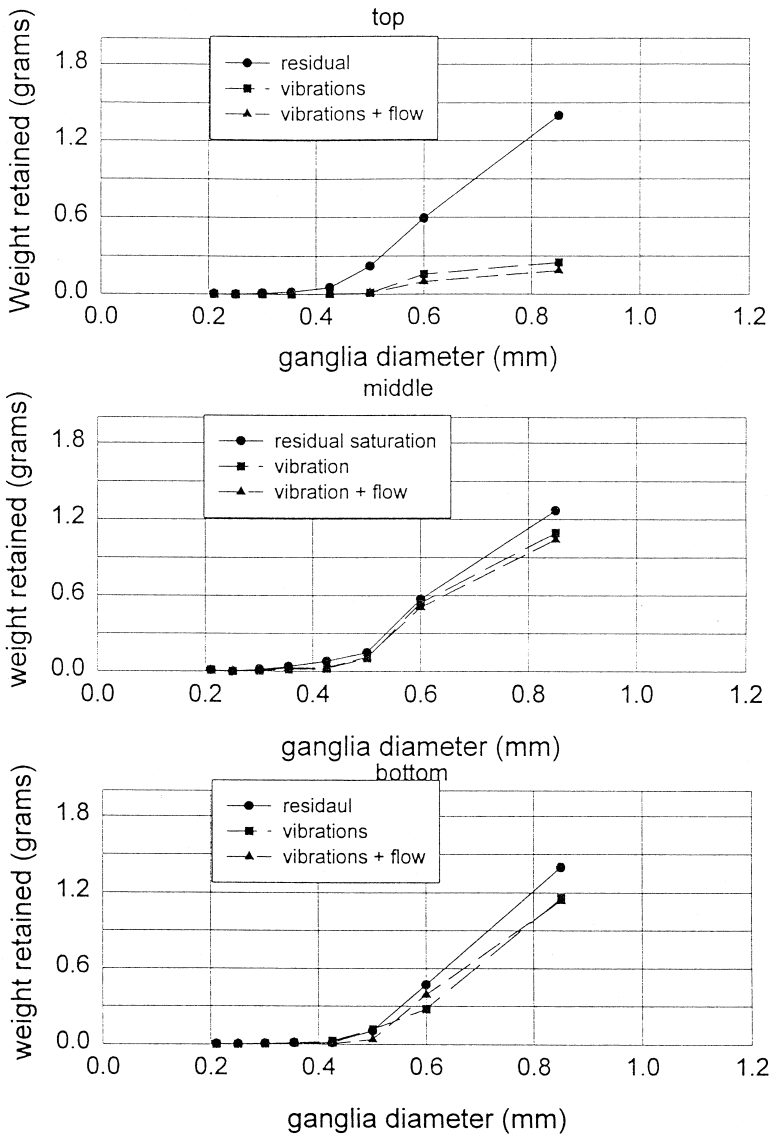

Fig. 12. Comparison of weights of ganglia trapped under different conditions in the top, middle, and bottom sections of the column.

section of the column was influenced more than the bottom and middle sections (Fig. 13). The relative differences in the entrapment between the top and bottom of the column were again attributed to the overburden stress which restricted the freedom of particle movement at greater depths. Figs. 12 and 13 also show that there was no significant difference in ganglia mobilization when simultaneous flow was created during vibrations. For the given porous media and the immiscible phase, the capillary

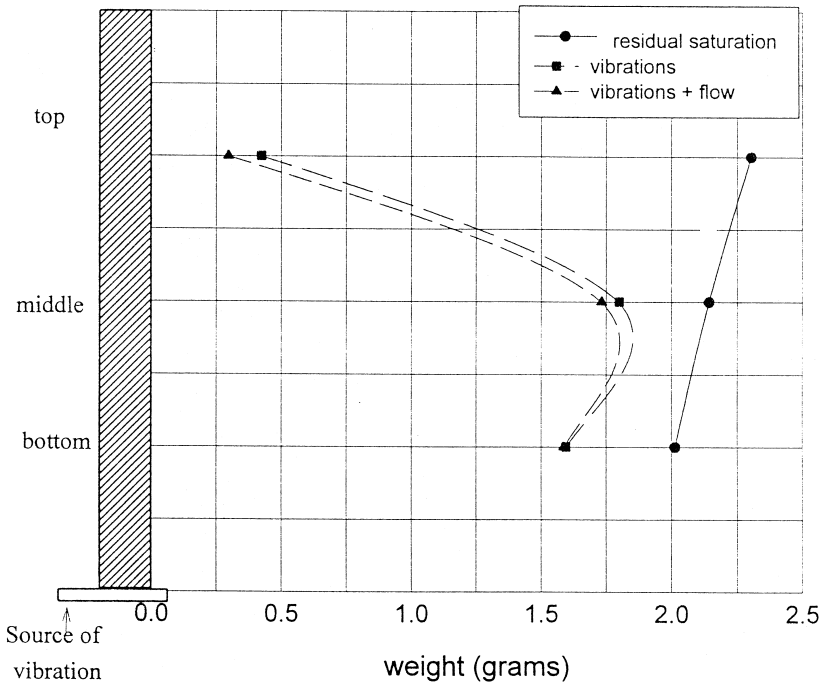

Fig. 13. Variation of ganglia entrapment with depth under different conditions.

numbers required to mobilize the residual ganglia with viscous force alone were in the range of 10^{-5} to 10^{-3} [12,13]. In these experiments, the capillary number was of the order of 10^{-6} which was therefore not sufficient to mobilize the ganglia.

The size distributions of ganglia trapped in the column showed no apparent differences between the three test conditions nor between the top, middle, and the bottom thirds of the column. Although break-up and coalescence of individual ganglia might be occurring within the soil column as a result of vibrations, the size distribution of the population seemed to be unaltered. Ng and Payatakes [14] suggested from their network modeling studies that a mobilized solitary ganglion is destined to either get stranded or to break up in a relatively few pore spaces, no more than thirty to fifty rheons (a rheon was defined as a single-step sudden leap taken by the ganglion in the general downstream direction). Thus, the processes of break-up and coalescence might be occurring only locally, over short distances, and the combined effect of these processes was not affecting the population's distribution over the scale of the column.

4. Conceptual framework for modeling ganglia transport under the influence of vibrations

In this section, we provide a mathematical basis for simulating ganglia transport under the influence of vibrations. Considering a monosized ganglia population dis-

tributed uniformly in a one-dimensional domain, the governing equation for the number of moving ganglia may be expressed as

$$\frac{\partial n}{\partial t} + u_z \frac{\partial n}{\partial z} = -nu_z[\lambda + \phi] \tag{1}$$

where n = number of moving ganglia; u_z = mean velocity of the moving ganglia; z, t = space and time dimensions, respectively; and λ, ϕ = stranding and break-up coefficients, respectively, of the monosized ganglia, and were defined by [16]

$$\left.\frac{\partial n}{\partial z}\right|_{\text{due to stranding}} = -\lambda n \tag{2}$$

$$\left.\frac{\partial n}{\partial z}\right|_{\text{due to breakup}} = -\phi n \tag{3}$$

The governing equation for the number of entrapped ganglia may be written similarly as

$$\frac{\partial \sigma}{\partial t} = nu_z \lambda \tag{4}$$

Eqs. (1) and (4) represent simplified conditions with the following processes not accounted for: i) flux of ganglia due to axial dispersion, ii) loss of moving or stranded ganglia due to collision/coalescence with other moving and stranded ganglia, and iii) generation of additional moving or stranded ganglia through collision/coalescence of smaller moving ganglia with stranded ones. Ng and Payatakes [14] showed that the coefficient of stranding (λ) and break-up (ϕ) can be expressed as

$$\lambda = -\frac{S}{(1-M)} \frac{\ln M}{s_z} \tag{5}$$

and

$$\phi = -\frac{B}{(1-M)} \frac{\ln M}{s_z} \tag{6}$$

where M, B, S = probability of mobilization, break-up, and stranding of a solitary ganglion, respectively, (therefore, $M + B + S = 1$), which could be obtained using a network model [14], and s_z = expected length of travel of the centroid of the ganglion per rheon.

At the wetting front, $z = Vt$ (where V = darcy velocity of water), in the one-dimensional domain, the number of moving and trapped ganglia may be expressed as

$$n = \frac{V\beta(1-S)}{V-u_z};\ \sigma = \beta S \qquad \text{for } t > 0 \tag{7}$$

where β = a coefficient representing the spatial heterogeneity in the distribution of initially stranded ganglia in the domain, which is a function of the spatial dimension z. Eq. (7) forms the boundary condition at the wetting front and assumes that the ganglia move in the direction of the wetting front at their own velocity. Although the ganglia

keep up with the water front for a little while, they immediately start to lag behind the front, eventually becoming stranded. Another front may be defined at $z = u_z t$, where the number of moving ganglia is given by $\beta(1 - S)$. In the region, $z \le u_z t$, all the ganglia are stranded, therefore $n = 0$. Thus, only the region, $u_z t < z < Vt$, contains moving ganglia.

As seen in Sections 2 and 3, the overburden stress has a dominant effect on the mobilization of ganglia. The effect of the overburden stress may be incorporated in the above framework by making λ and ϕ spatially dependent. Assuming that overburden stress decreases with spatial dimension z, we treat λ as an exponentially-decaying function with respect to z, or

$$\lambda = \lambda_0 e^{-\alpha z} \tag{8}$$

where $\lambda_0 =$ coefficient of stranding at $z = 0$ where the overburden stress is the maximum and therefore, the effect of vibrations is minimal or non-existent, and $\alpha =$ a coefficient representing the decrease in the likelihood of stranding as a result of increased momentary particle arrangement during vibrations.

In order to demonstrate the best possible recoveries due to vibrations and to simplify the presentation of the analytical solutions, the break-up coefficient, ϕ, is set to zero. Thus, $S + M = 1$. λ and S are related through Eq. (5) which now simplifies to

$$\lambda(z) = -\frac{\ln[1 - S(z)]}{s_z} \tag{9}$$

or

$$S(z) = -\exp[-\lambda_0 s_z e^{-\alpha z}] \tag{10}$$

Using the method of characteristics [5,6], the solution to Eq. (1) with boundary condition given in Eq. (7) may be expressed as

$$n = \frac{V\beta}{V - u_z}\exp\left\{\lambda_0(s_z - \alpha)\exp\left[\frac{-\alpha V(u_z t - z)}{(u_z t - V)}\right]\right\}\exp(\alpha\lambda_0 e^{-\alpha z}) \tag{11}$$

The number of stranded ganglia may be obtained similarly by solving Eq. (4) with the boundary condition, $\sigma(z) = \beta S(z)$ at $z = Vt$. This requires integration of exponential terms, and because of the nature of Eq. (11), closed form expressions for integration are not available. Truncation of the higher order terms in series expansion of the exponential function yields the solution for σ as

$$\frac{\sigma - \beta\{1 - \exp(-\lambda_0 s_z e^{-\alpha Vt})\}}{\lambda\beta/\alpha} = \left\{\begin{array}{l} \exp[\lambda_0 \alpha e^{-\alpha z}]\left[\ln x + yx + \dfrac{(xy)^2}{4} + \dfrac{(xy)^3}{18}\right] \\ -\exp[\lambda_0 \alpha e^{-\alpha Vt}]\left[(-\alpha Vt) + ye^{-\alpha Vt} + \dfrac{(e^{-\alpha Vt})^2 y^2}{4} + \dfrac{(e^{-\alpha Vt})^3 y^3}{18}\right] \end{array}\right\} \tag{12}$$

where

$$y = -\lambda_0(s_z + \alpha) \tag{13}$$

Eqs. (11) and (12) together give the number of moving and stranded ganglia in a soil column subjected to vibrations. Note that break-up and coalescence processes are not incorporated in this formulation, and as such it represents an approximate solution. To demonstrate the nature of the solution, the number of entrapped ganglia in a soil column subjected to vibrations are plotted against z in Fig. 14 for some hypothetical values of parameters involved. Although the soil column was devoid of entrapped ganglia at large values of z (where the overburden stress decreases and consequently the probability of stranding S is less), the ganglia mobilized at the bottom were accumulated at small values of z, and the front of accumulated ganglia entrapment progressed with time. This, in general, conformed with the experimental observations made in the second part of this paper (Fig. 13).

A thorough validation of the conceptual framework described above was not possible because of the number of parameters involved, which could not be readily obtained from the qualitative results of the experimental programs described earlier. However, it is useful to present the sensitivity of the solution to some important parameters. The variations in the number of entrapped ganglia in the zone $u_z t < z < Vt$, as λ_0, α, and u_z were varied (Fig. 15). Note that the maximum number of entrapped ganglia occurs at

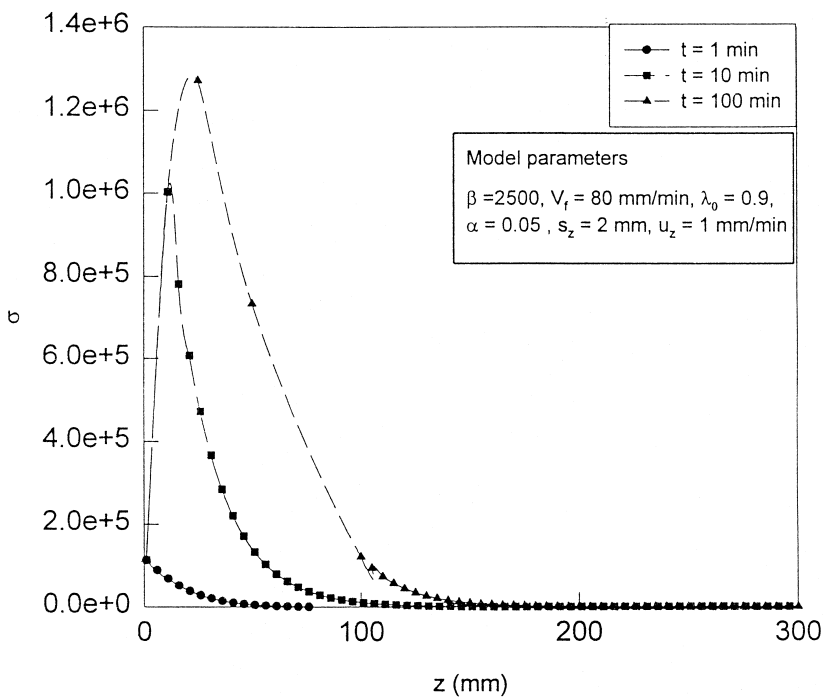

Fig. 14. Trends of ganglia entrapment at various times predicted for a hypothetical set of parameters.

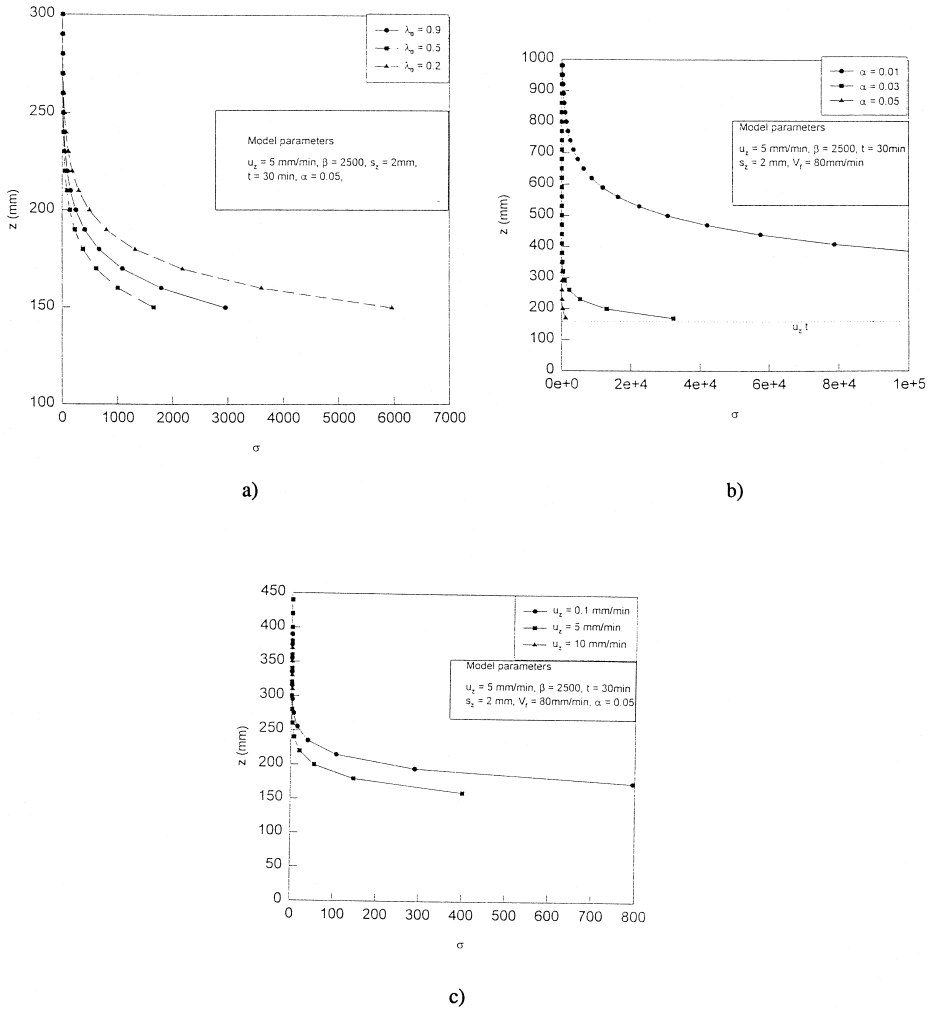

Fig. 15. Effect of a) stranding coefficient, λ_0, at $z = 0$, b) exponential function coefficient, α, and c) mean velocity of the moving ganglia, u_z, on ganglia entrapment.

$z = u_z t$ at any given time t. A reduction in λ_0 signified a reduction in stranding probabilities causing less number of entrapped ganglia throughout the column (Fig. 15a). Similarly, α indicates the attenuation of stranding coefficients with respect to z; at large values of α, the stranding probabilities are less at a given z. Thus, the entrapment is in general less for large values of α (Fig. 15b). As seen in Fig. 15c, larger values of u_z result in less entrapment in the region under consideration. This is because, at a large value of u_z and for a given time t, the region $u_z t < z < Vt$ is situated at a higher location in the soil column where, because of the variation of the stranding coefficient, the entrapment is less.

It should be reiterated that the above formulation should serve as a conceptual framework, and it is adequate for qualitative evaluations only. For accurate prediction of the ganglia entrapment during vibrations, the nature and magnitude of parameters involved in the formulation should be determined systematically.

5. Summary and conclusions

The pore-scale movement of a solitary ganglion and that of a population of ganglia, under the influence of vibrations, is quantitatively evaluated using results from a micromodel and soil column experiments. The micromodel experiments enabled a direct visualization of momentary particle arrangement during vibrations. A 20- to 30-fold momentary increase in the interparticle spacing was observed in these experiments. Blobs of Soltrol introduced into the porous media underwent break-up and coalescence processes during vibrations. Larger amplitudes enhanced the mobility of ganglia. At greater depths, however, the overburden stress restricted the momentary particle arrangement and the ganglia remained immobilized.

Column experiments using Hexadecane as the LNAPL confirmed this role of overburden stress. Analyses on solidified Hexadecane ganglia from vibrated columns indicated better mobilization of ganglia from top of the column (where overburden stress is less) than from bottom of the column. The size distributions of ganglia did not reflect significant differences between the top, middle, and bottom sections of the column. No noticeable differences in size distribution were observed as a result of vibrations. This implied that the break-up and coalescence processes occurring during vibrations were local, and their combined effect on the size distribution of ganglia population was insignificant.

A mathematical framework was conceived to represent the effect of vibrations on ganglia transport. An advection-type equation was used to simulate the transport with ganglia stranding included as a sink term. The effect of overburden stress was taken into account by conceptualizing stranding as space-dependent. Using the method of characteristics, the solutions for moving and stranded ganglia in a soil column subjected to vibrations were developed for the simple case where break-up and coalescence were absent. Only a qualitative picture of ganglia transport was possible with this formulation because of the requirement of a number of parameters even with the simplifying assumptions involved. The authors hope that this study provides impetus for more comprehensive research efforts in the future so that a predictive capability for vibratory mobilization of residual ganglia can be developed.

Acknowledgements

The work presented in this paper is part of a project funded by the National Science Foundation under Grant MSS-9209425. The support provided by this agency is gratefully acknowledged. The writers also thank the anonymous reviewers for their helpful comments.

References

[1] R.E. Brown, Vibroflotation compaction of cohesionless soils, ASCE Journal of Geotechnical Engineering Division 103 (12) (1977) 1437–1451.
[2] I. Chatzis, N.R. Morrow, H.T. Lim, Magnitude and detailed structure of residual oil saturation, Society of Petroleum Engineers Journal, April 1983, SPE 10681, pp. 311–326.
[3] S.H. Conrad, J.L. Wilson, W.R. Mason, W.J. Peplinski, Visualization of residual organic liquid trapped in aquifers, Water Resources Research 28 (2) (1992) 467–478.
[4] E. D'Appolonia, L.E. Miller Jr., T.M. Ware, Sand compaction by vibroflotation, Proceedings of ASCE 79 (200) (1953) 1–23.
[5] R. Haberman, Elementary Applied Partial Differential Equations, 2nd edn., Prentice-Hall, Englewood Cliffs, NJ, 1987.
[6] F.B. Hildebrand, Advanced Calculus for Applications, 2nd edn., Prentice-Hall, Englewood Cliffs, NJ, 1976.
[7] V. Hornof, N.R. Morrow, Flow visualization of the effects of interfacial tension on displacement, SPE Reservoir Engineering, February 1988, pp. 251–256.
[8] M.I. Lowry, C.T. Miller, Pore-scale modeling of nonwetting-phase residual in porous media, Water Resources Research 31 (3) (1995) 455–473.
[9] A.S. Mayer, C.T. Miller, The influence of porous medium characteristics and measurement scale on pore-scale distributions of residual nonaqueous-phase liquids, J. Contam. Hydrol. 11 (3–4) (1992) 189–213.
[10] A.S. Mayer, C.T. Miller, An experimental investigation of pore-scale distributions of nonaqueous phase liquids at residual saturation, Transp. Porous Media 10 (1) (1993) 57–80.
[11] J.W. Mercer, R.M. Cohen, A review of immiscible fluids in the subsurface: properties, models, characterization and remediation, Journal of Contaminant Hydrology 6 (1990) 107–163.
[12] N.R. Morrow, I. Chatzis, Measurement and correlation of conditions for entrapment and mobilization of residual oil. Report DOE/BC/10310-20, Department of Energy, Washington, DC, 1982.
[13] N.R. Morrow, I. Chatzis, J.J. Taber, Entrapment and mobilization of residual oil in bead packs, SPE Reservoir Engineering 3 (3) (1988) 927–934.
[14] K.M. Ng, A.C. Payatakes, Stochastic simulation of the motion, breakup and stranding of oil ganglia in water-wet granular porous media during immiscible displacement, AIChE Journal 26 (3) (1980) 419–429.
[15] A.C. Payatakes, Dynamics of oil ganglia during immiscible displacement in water wet porous media, Annu. Rev. of Fluid Mech. 14 (1982) 365–393.
[16] A.C. Payatakes, K.M. Ng, R.W. Flumerfelt, Oil ganglion dynamics during immiscible displacement: model formulation, AIChE Journal 26 (3) (1980) 430–443.
[17] S.E. Powers, L.M. Abriola, W.J. Weber Jr., An experimental investigation of nonaqueous phase liquid dissolution in saturated subsurface systems: steady state mass transfer rates, Water Resources Research 28 (10) (1992) 2691–2705.
[18] L.N. Reddi, Feasibility of in situ implementation of vibrations to mobilize NAPL ganglia, Journal of Soil Contamination 3 (1) (1994) 29–46.
[19] L.N. Reddi, S. Challa, Vibratory mobilization of immiscible liquid ganglia in sands, ASCE Journal of Environmental Engineering 120 (5) (1994) 1170–1190.
[20] L.N. Reddi, H. Wu, Mechanisms involved in vibratory destabilization of NAPL ganglia in sands, ASCE Journal of Environmental Engineering 122 (12) (1996) 1115–1119.
[21] J.L. Wilson, S.H. Conrad, W.R. Mason, W. Peplinski, Laboratory investigation of residual liquid organics from spills, leaks, and the disposal of hazardous wastes in groundwater, EPA/600/6-90/004, Washington, DC, 1990.
[22] G.D. Yadav, F.A.L. Dullien, I. Chatzis, I.F. MacDonald, Microscopic distribution of wetting and nonwetting phases in sandstones during immiscible displacements, SPE Reservoir Engineering, May 1984, 1987, pp. 137–144.